

# Surface-wave suppression band gap and plane-wave reflection phase band of mushroomlike photonic band gap structures

Long Li,<sup>1,a)</sup> Qiang Chen,<sup>2</sup> Qiawei Yuan,<sup>3</sup> Changhong Liang,<sup>4</sup> and Kunio Sawaya<sup>2</sup>

<sup>1</sup>National Laboratory of Antennas and Microwave Technology, Xidian University, Xi'an 710071, China and Department of Electrical and Communication Engineering, Tohoku University, Sendai 980-8579, Japan

<sup>2</sup>Department of Electrical and Communication Engineering, Tohoku University, Sendai 980-8579, Japan

<sup>3</sup>Department of Electrical and Electronic Engineering, Tokyo University of Agriculture and Technology, Tokyo, 184-8588, Japan

<sup>4</sup>National Laboratory of Antennas and Microwave Technology, Xidian University, Xi'an 710071, People's Republic of China

(Received 3 July 2007; accepted 14 November 2007; published online 23 January 2008)

Mushroomlike photonic band gap (PBG) structures exhibit two band gap characteristics: surface-wave suppression and in-phase reflectivity. The fundamental electromagnetic properties and the relationship between the surface-wave suppression band gap and the plane-wave reflection phase band are investigated and clarified by a finite-element full-wave analysis. The results of the plane-wave bistatic reflection experiments on mushroomlike PBG plates in an anechoic chamber are in good agreement with those of numerical simulation, confirming the phenomenon of dual in-phase reflection, i.e., dual-resonant behavior, for a transverse magnetic polarization plane wave at oblique incidence on a mushroomlike PBG surface. A modified local resonance cavity cell model of a PBG structure is presented to provide insight into the physical mechanism of dual-resonant behavior.

© 2008 American Institute of Physics. [DOI: 10.1063/1.2832401]

## I. INTRODUCTION

Artificial electromagnetic materials, such as photonic band gap (PBG) structures,<sup>1,2</sup> photonic crystals,<sup>3</sup> and left-handed materials,<sup>4,5</sup> are broadly classified as metamaterials, which are typically created using two- or three-dimensional periodic metallic and dielectric structures.<sup>6,7</sup> They have attracted significant research interest in recent years due to their special electromagnetic properties, which are applicable to a wide range of electromagnetic devices. This paper focuses on a two-dimensional mushroomlike PBG structure<sup>7</sup> with planar periodic square patches connected to a dielectric substrate ground by vertical posts or metal-plated vias, as shown in Fig. 1. Compared with other PBG structures such as dielectric rods and holes, this structure has the advantage of compactness, which is important in communication antennas and arrays. The physical mechanism of the mushroomlike PBG structure can be simply explained from the viewpoint of an LC parallel resonant circuit. The local resonant behavior provides high-impedance reflectivity and prevents the propagation of radio-frequency surface currents along the structure.<sup>7,8</sup> Its band gap features are revealed in two ways: the suppression of surface-wave propagation and an in-phase reflection coefficient. The surface-wave suppression improves antenna performance by, for example, increasing the antenna gain, reducing the back radiation, and eliminating the scan blindness in phased arrays.<sup>7-11</sup> The in-phase reflection coefficient enables the design of artificial magnetic conductors and low-profile antennas.<sup>12,13</sup> It is well-known that a perfect electric conductor (PEC) has a 180° reflection phase, while a perfect magnetic conductor (PMC), which does not

exist in nature, has a reflection phase of 0°. The reflection phase of the PBG surface varies continuously from 180° to -180° versus frequency. Near the high-impedance resonance, a plane wave is reflected in-phase (between +90° and -90°) rather than out-of-phase, as occurs on a PEC surface. This can produce the PMC-like condition in a certain frequency band.

An important question arises: what is the relationship between the surface-wave suppression band gap and the plane-wave in-phase reflection band? Sievenpiper *et al.*<sup>7</sup> sug-

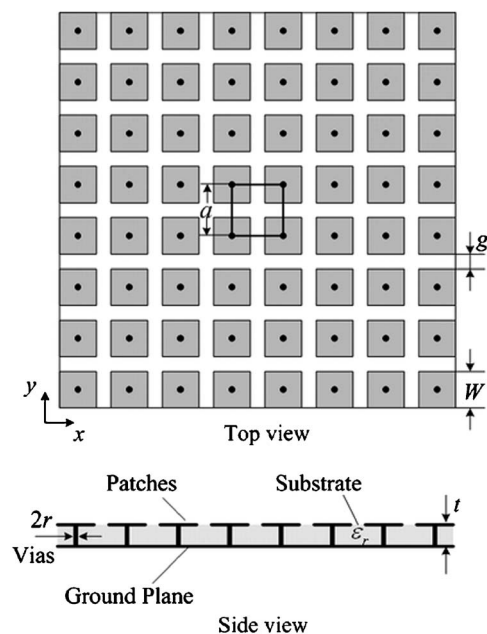


FIG. 1. Geometry of mushroomlike PBG structure.

<sup>a)</sup>Electronic mail: lilong@mail.xidian.edu.cn; lilong@ecei.tohoku.ac.jp.

gested that the in-phase reflection frequency band generally corresponds to the range of the surface-wave band gap. Yang and Rahmat-Samii<sup>13</sup> pointed out that a reflection phase in the range of  $90^\circ \pm 45^\circ$  could be used to identify the input-match frequency band of a low-profile wire antenna. The operating frequency band is an overlap of the input-match frequency band and the surface-wave band gap. Clavijo *et al.*<sup>14</sup> used a two-layer anisotropic uniaxial effective medium model of the PBG structure to show that the surface-wave suppression results from the unusual axial constitutive properties of the material, and that the surface-wave band gap edges are not necessarily correlated with the  $+90^\circ$  and  $-90^\circ$  phase-shift points of the reflection coefficient. Tretyakov and Simovski<sup>15</sup> developed an analytical dynamic model of the electromagnetic properties of such a PBG structure and used a reflection phase band in the range of  $\pm 90^\circ$  to determine the surface-wave band gap. Saville used a focused beam system to investigate conformal high-impedance PBG ground planes, and used the linear region of the reflection phase from  $+45^\circ$  to  $-45^\circ$  to identify the surface-wave suppression band gap.<sup>16</sup> Although the results of these studies are not in complete agreement, they do show that the relationship between the surface-wave suppression band gap and the plane-wave reflection phase band is very complex.

In this paper, we report our numerical and experimental results for the electromagnetic characteristics of and the relationship between the surface-wave suppression band gap and the plane-wave in-phase reflection band. The present work differs from previous investigations in several ways. The characteristics of the two bands were separately investigated using the same full-wave analysis model. The effects of each parameter on the two bands were investigated to clarify the complex relationship. The dual in-phase reflection that occurs when a transverse magnetic polarization plane wave obliquely illuminates the PBG structure is validated by theoretical simulations and experiments. A modified local resonance cavity cell (MLRCC) model of PBG structures is presented to explain the essential characteristics of dual-resonant behavior and their angular and polarization dependences.

## II. TWO BAND GAP CHARACTERISTICS OF MUSHROOMLIKE PBG STRUCTURES

The surface-wave band gap and the reflection phase of mushroomlike PBG structure are mainly determined by five characteristic parameters (see Fig. 1): patch width ( $W$ ), gap width ( $g$ ), thickness ( $t$ ), via radius ( $r$ ), and substrate permittivity ( $\epsilon_r$ ). The period of the PBG structure is  $a=W+g$ . An infinite periodic structure (shown in Fig. 2), i.e., a single cell with periodic boundary conditions (PBCs) on four sides, was used to analyze the effects of the five parameters on the two bands separately. The initial parameter values were

$$W = 0.14\lambda_6 \text{ GHz},$$

$$g = 0.006\lambda_6 \text{ GHz},$$

$$t = 0.03\lambda_6 \text{ GHz},$$

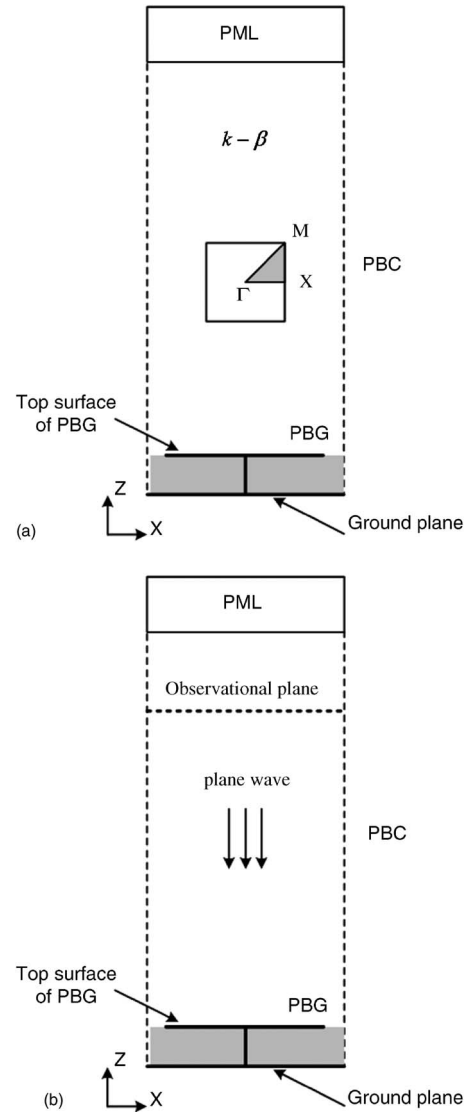


FIG. 2. Infinite periodic models based on finite element algorithm used for (a) calculating dispersion diagram in irreducible Brillouin zone and (b) calculating reflection phase of plane wave at normal incidence, in which periodic boundary conditions (PBCs) are placed around PBG cell to model infinite PBG surface.

$$r = 0.01\lambda_6 \text{ GHz},$$

and

$$\epsilon_r = 2.65, \quad (1)$$

where  $\lambda_6 \text{ GHz}$  is the free-space wavelength at 6 GHz, which is used as a reference length to define the physical dimensions of the various PBG structures studied in this paper. Figure 3(a) shows the numerically simulated  $k-\beta$  dispersion diagram of the surface modes propagating in the PBG structure. The simulation was done using a finite-element full-wave analysis<sup>17</sup> and the computational model shown in Fig. 2(a);  $k=\omega/c$  is the free-space wave number, and  $\beta$  is the surface-wave propagation constant. The first (dominant) surface-wave mode is the transverse magnetic (TM) mode, which has no cutoff frequency; the second is the transverse electric (TE) mode. There was a complete stopband between the first mode,  $TM_0$ , and the second mode,  $TE_1$ , in the fre-

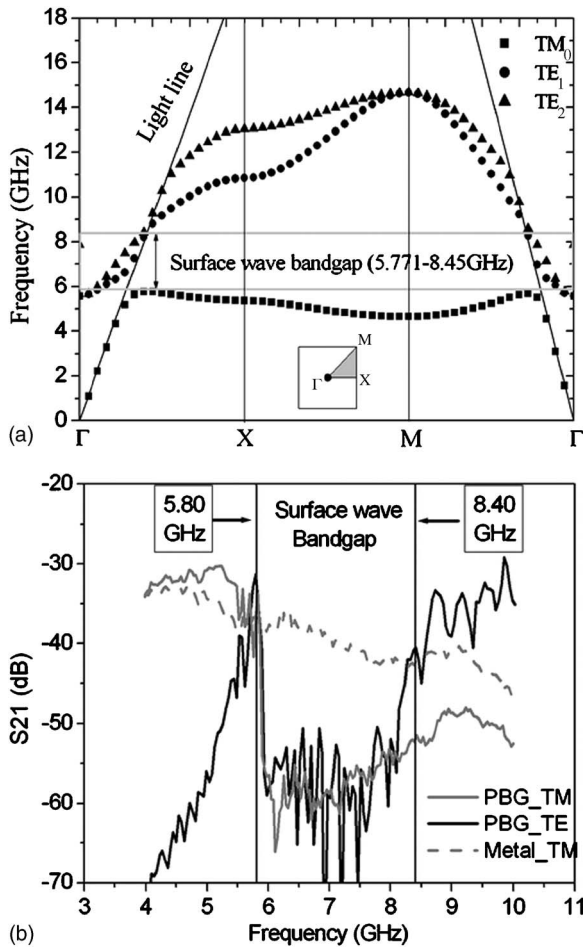


FIG. 3. Measurement and simulation of surface-wave band gap of PBG structure: (a) simulated surface-wave band structure; (b) measured TM and TE surface-wave transmission coefficients for PBG structure, including transmission characterization of TM surface wave in metal surface of same size as tested PBG sample ( $20 \times 20$  unit cells;  $146 \times 146$  mm).

quency band 5.771–8.45 GHz. In this figure,  $\Gamma$ ,  $X$ , and  $M$  represent the symmetric points of the irreducible Brillouin zone. The  $\Gamma$ – $X$  branch represents  $\beta_x a / \pi$  with  $\beta_y = 0$ , the  $X$ – $M$  branch represents  $\beta_y a / \pi$  with  $\beta_x = \pi / a$ , and the  $M$ – $\Gamma$  branch represents  $\beta_x a / \pi$  with  $\beta_x = \beta_y$ . In this way, we spanned all possible wave vectors in the  $x$  and  $45^\circ$  directions, and we also spanned two special points (the minimum and maximum wave vectors) in the other directions. Calculation inside this special Brillouin zone provides sufficient surface-wave band gap information. Figure 3(b) shows the frequency response of the transmission coefficient  $S_{21}$ , where both TM and TE surface waves were measured by using a pair of small monopole antennas oriented vertically (TM mode) and a pair of small shielded loop antennas oriented parallel (TE mode) to the PBG surface,<sup>7</sup> respectively. The simulated surface-wave band gap was in good agreement with the measured result.

The reflection phase band generally depends not only on the PBG structure itself but also on the incident angle and polarization of a plane wave. The element of a conventional PBG structure is a square patch that is symmetric in the  $x$  and  $y$  directions, as shown in Fig. 1. The reflection phases are thus independent of the polarization for normally inci-

dent plane waves, which are stable and can be used to identify the surface-wave band gap features.<sup>7,13</sup> In the model used for calculating the reflection phase of plane waves at normal incidence [Fig. 2(b)], the observational plane was set in the far-field zone of the PBG surface. A perfectly matched layer (PML) was positioned to absorb the reflection waves. The scattered  $E$ -field on the observational plane was recorded, and the reflection phase at this plane was calculated using

$$\phi_{\text{PBG}} = \frac{\int_S \text{phase}(E_{\text{scattered}}) ds}{\int_S \hat{s} \cdot d\vec{s}}, \quad (2)$$

where  $S$  is the evaluation surface and  $\hat{s}$  is its normal unit vector. For reference, the scattered  $E$ -field from a PEC surface was also calculated. The PEC surface was made coincident with the PBG top surface, while the observational reflection plane was left the same. A factor of  $\pi$  was added to the phase to account for the reference of the PEC surface, which is known to have a phase shift of  $\pi$  radians.

Parametric studies were performed to identify the effects of the PBG structure parameters on the two bands and on their relationship. Figures 4(a)–4(e) show the surface-wave band gap and the reflection phase of a plane wave normally incident on the PBG surface for different patch widths, gap widths, substrate thicknesses, permittivities, and via radii, respectively. Note that when the value of a parameter was changed, such as when the patch width was changed from  $0.04\lambda_6$  GHz to  $0.20\lambda_6$  GHz, the values of the other parameters were kept the same as in Eq. (1). The frequency range between two circles on each curve in Fig. 4 represents the position of the surface-wave suppression band gap of the corresponding PBG structure, which was calculated by simulating dispersion diagrams. The electromagnetic properties and the relationship between the two bands were obtained from these results.

- (1) The surface-wave band gap was not necessarily related to the in-phase reflection band. The corresponding relationship between the two bands varied with the parameter values, especially for a significant change in the TM surface-wave band edge.
- (2) The variations in the characteristics of the two bands with the parameter values were almost the same, meaning that we can predict the effects of PBG parameters on the position and bandwidth of the surface-wave suppression band gap by using their effects on the position and slope of the in-phase reflection band.
- (3) The metal vias play an important role in determining the surface-wave suppression band gap. As shown in Figs. 4(e) and 4(f), although there was no band gap in the surface-wave suppression for the via-less structure, there was still an in-phase reflection band. The reflection phase characteristics were barely changed when the via radius was much less than the patch width. However, when the radius was increased, the reflection phase band

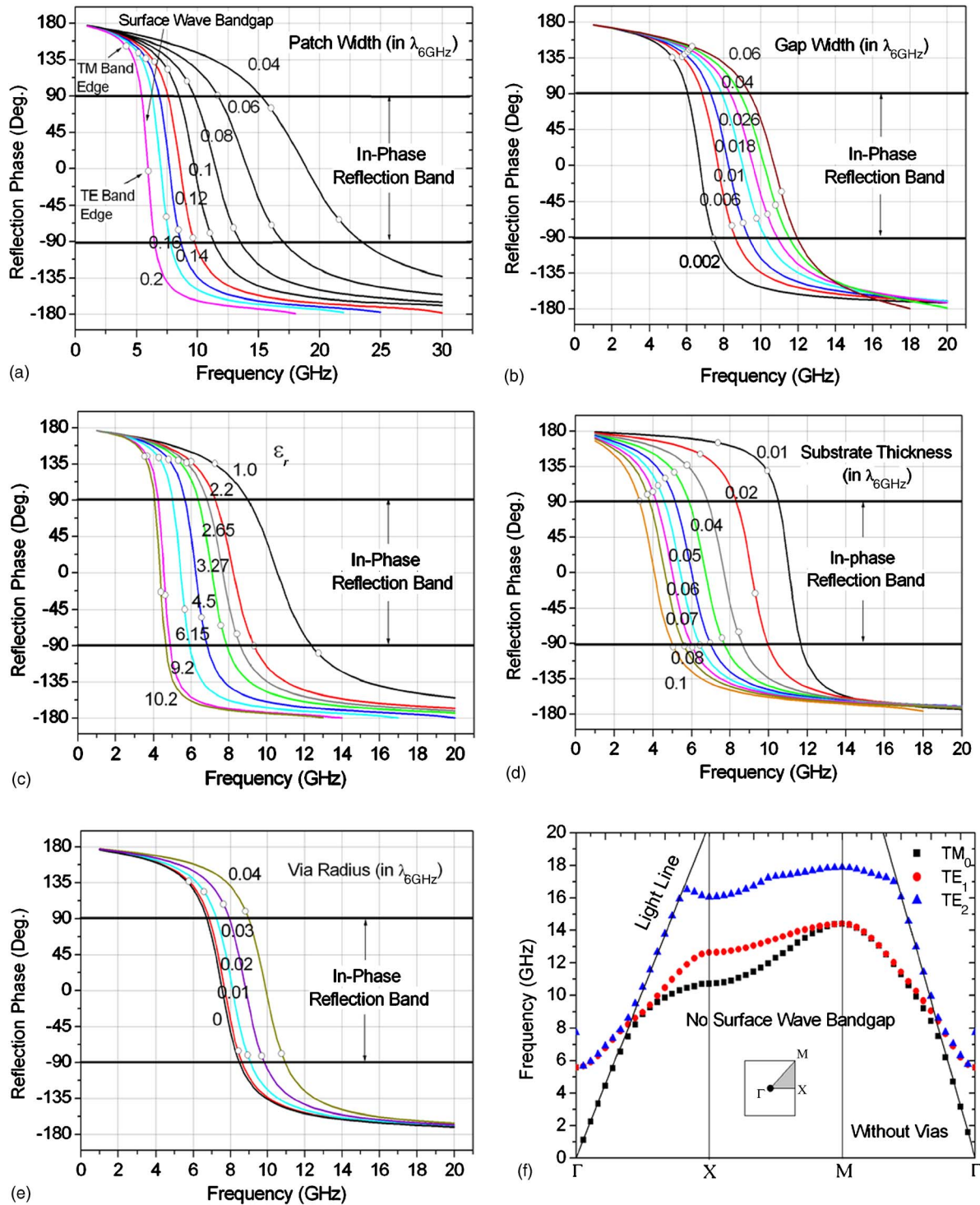


FIG. 4. (Color online) Parametric analyses and corresponding relationships between two bands of PBG structures: (a) effect of changing patch width from  $0.04\lambda_{6\text{ GHz}}$  to  $0.20\lambda_{6\text{ GHz}}$ ; (b) gap width from  $0.002\lambda_{6\text{ GHz}}$  to  $0.06\lambda_{6\text{ GHz}}$ ; (c) permittivity from 1.0 to 10.2; (d) substrate thickness from  $0.01\lambda_{6\text{ GHz}}$  to  $0.1\lambda_{6\text{ GHz}}$ ; and (e) via radius from 0 to  $0.04\lambda_{6\text{ GHz}}$ , while keeping other parameters unchanged. (f) Dispersion diagram of PBG structure without vias, which indicates that there is no surface-wave suppression band gap in the structure. Note that the frequency region between two circles on each curve represents the position of surface-wave suppression band gap of the corresponding PBG structure.

increased and its bandwidth decreased due to the coupling between the metal vias and the gap between adjacent patches. Moreover, the edge of the TM surface-wave band gradually approached the frequency point of  $+90^\circ$  reflection phase with an increase in via radius.

- (4) The correspondence between the two bands can be effectively adjusted by changing the ratio of the period to

the thickness  $a/t$ , assuming  $r$  is kept small. Numerical tests showed that, when  $a/t < 2$ , the surface-wave band gap was between the  $\pm 90^\circ$  reflection phase frequencies for normal incidence. In practice, it is highly desirable to find a material that simultaneously shows in-phase reflection and a surface-wave band gap in a certain frequency band.

The interaction between the metal patch and the ground plane can be viewed as far-zone interaction when the substrate thickness  $t$  is large compared to period  $a$  of a PBG structure, even if  $t$  and  $a$  are small compared to the operating wavelength.<sup>18</sup> This means that we need to consider only the fundamental-mode plane wave between the array and the ground, which leads to the transmission-line formula for the equivalent surface impedance of the PBG structure. However, if  $t$  is smaller than  $a$ , we need to take into account the effect of higher-order evanescent modes reflected by the ground plane. The effect factor of the evanescent modes can be expressed simply as<sup>15</sup>

$$\gamma = \frac{2a}{\lambda} \log(1 - e^{-(4\pi t/a)}) < 0, \quad (3)$$

$(a \ll \lambda).$

When  $a \ll \lambda$  is not satisfied, the effect factor can be expressed using a convergent series,<sup>19</sup>

$$\gamma = \frac{2a}{\lambda} \sum_{m=1}^{\infty} \left( \frac{1 - e^{-4\pi(t/a)\sqrt{m^2 - (a/\lambda)^2}}}{\sqrt{m^2 - (a/\lambda)^2}} - \frac{1}{m} \right). \quad (4)$$

It can be seen that the higher-order evanescent mode influence is negligible if  $t \approx a/2$ , which is consistent with our numerical results. When  $a/t < 2$ , the plane-wave in-phase reflection band generally corresponds to the surface-wave suppression band gap. Reviewing a PBG structure consisting of a triangular array of hexagonal patches, as proposed by Sievenpiper,<sup>7</sup> with  $a/t = 2.54/1.55 \approx 1.639$ , we see that the surface-wave band gap edges occur where the reflection phase is equal to  $\pm 90^\circ$ . If  $a/t$  is increased ( $>2$ ), the band edge of a TM surface wave gradually deviates from the frequency point of the  $\pm 90^\circ$  reflection phase and enters the out-of-phase region, as shown in Figs. 4(a) and 4(d). The square PBG structure of Yang<sup>13</sup> has  $a/t = 0.14/0.04 = 3.5$ , and the TM surface-wave band edge is approximately located at the frequency point of the  $138.1^\circ$  reflection phase. Our results show that the results of previous investigations<sup>7,13-16</sup> are reconcilable and that their primary differences are due to the different corresponding relationships for the two bands of mushroomlike PBG structures.

- (5) The relative permittivity of the substrate used to fabricate the PBG structure plays a less important role in adjusting the correspondence of the two bands, as shown in Fig. 4(c).

### III. DUAL-RESONANT BEHAVIOR FOR OBLIQUE INCIDENCE OF TM MODES ON MUSHROOMLIKE PBG STRUCTURES

As described above, a PBG structure with a square array of square patches is symmetric in the  $x$  and  $y$  directions. The reflection phase is independent of the polarization of a normally incident plane wave, which is stable and can be used to identify the band gap characteristics. However, when a plane wave obliquely illuminates the PBG surface, the phase of the reflected field depends on the incidence angle and

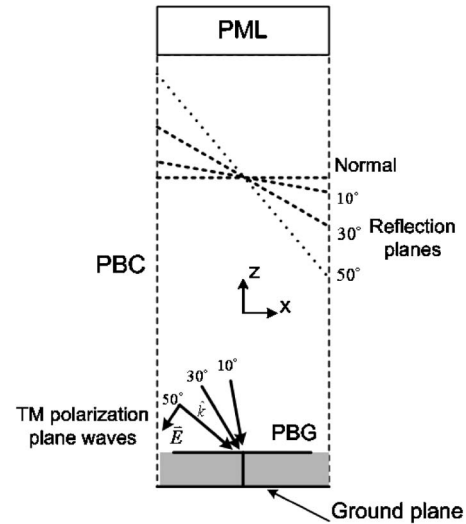
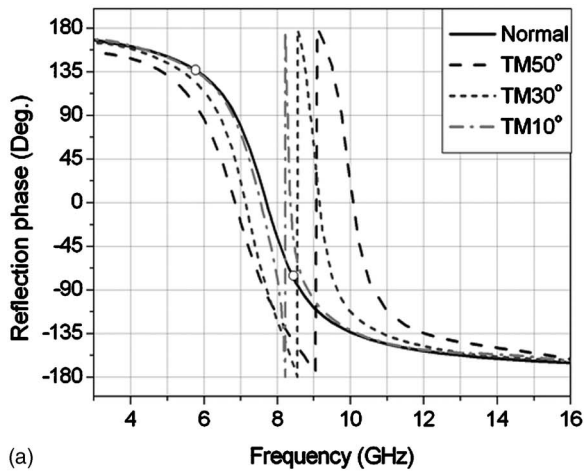


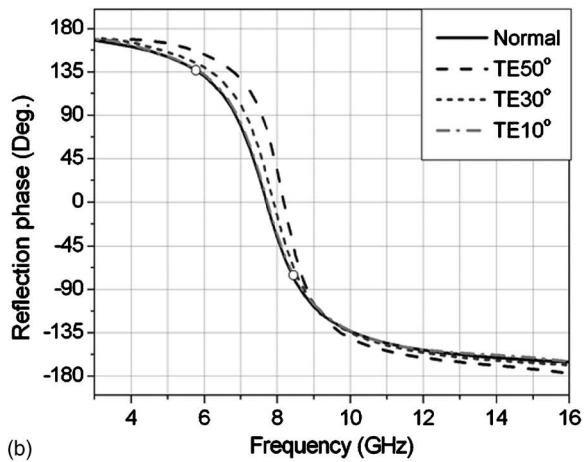
FIG. 5. Reflection-phase model for TM-polarized plane waves at oblique incidence on PBG surface at  $10^\circ$ ,  $30^\circ$ , and  $50^\circ$ .

polarization.<sup>20,21</sup> Figure 5 shows the oblique incidence model used for evaluating the reflection phase of the PBG surface. A TM polarization plane wave is launched to obliquely illuminate the PBG structure at  $10^\circ$ ,  $30^\circ$ , and  $50^\circ$ , respectively. The corresponding reflection planes are oblique with respect to the  $z$ -axis, and their centers are coincident to the observational plane at normal incidence.

Figure 6(a) shows the simulation results for the reflection phases of a TM-polarized plane wave at oblique incidence on a mushroomlike PBG structure. The frequency range between two circles represents the position of the surface-wave suppression band gap of the corresponding PBG structure. We can observe the presence of the dual in-phase reflection bands, i.e., the dual-resonant behavior. The first in-phase reflection frequency band is lower than that of the plane wave at normal incidence on the PBG structure and is located inside the surface-wave suppression band gap. The second in-phase reflection frequency band is higher and is located outside the surface wave suppression band gap. Moreover, as the incidence angle is increased, the two resonant frequency points of the zero-degree reflection phase deviate, and the slope of the phase response decreases. When a TE-polarized plane wave obliquely illuminates the PBG structure, the incident TE electric field is always parallel to the PBG surface, and the via conductors are not excited. Therefore, it is not necessary to take into account the metal vias. The model for calculating the reflection phase is the same as that in Fig. 5 except that the incident field is changed to TE polarization. Figure 6(b) shows the reflection phase characteristics of a TE-polarized plane wave at oblique incidences of  $0^\circ$  (normal),  $10^\circ$ ,  $30^\circ$ , and  $50^\circ$ . Only one in-phase reflection band can be observed, as with normal-incidence plane-wave excitation, but the resonant frequency and slope of the phase response increase with the incidence angle. To further clarify the effect of the metal vias on the dual in-phase reflection behavior, we analyzed the reflection-phase features of a TM-polarization plane wave obliquely illuminating the same PBG structure but without vias. As shown in Fig. 7(a), there was no dual in-phase reflection phenomenon.



(a)



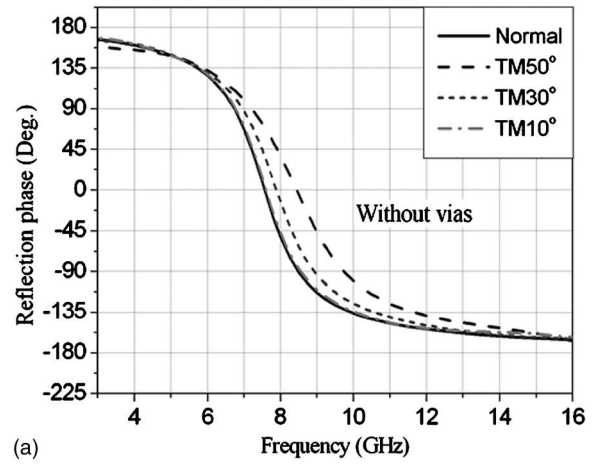
(b)

FIG. 6. Reflection-phase characteristics of plane wave at oblique incidence on PBG structure: (a) dual-resonant behavior of TM-polarized plane waves for oblique incidence; (b) single-resonant behavior of TE-polarized plane waves for oblique incidence.

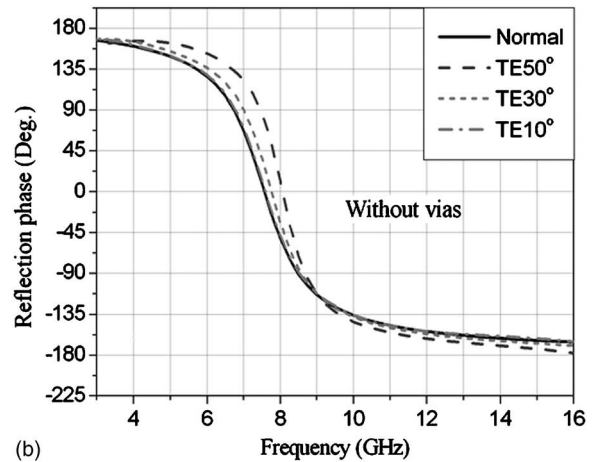
Only when the incidence angle of the TM plane wave was increased did the frequency band position increase, but the slope of the in-phase reflection band decreased. The reflection phases of a structure without vias were similarly calculated for a TE-polarized incident plane wave. A comparison between the results [Fig. 7(b)] and those shown in Fig. 6(b) clearly shows that the metal vias need not be considered for TE-polarization plane-wave incidence.

#### IV. A MODIFIED LOCAL RESONANCE CAVITY CELL MODEL OF PBG STRUCTURES

A modified local resonance cavity cell (MLRCC) model of PBG structures can be used to gain an insight into the dual-resonance behavior. We modified the LRCC model<sup>8</sup> by using its complementary model and replaced the PMC boundary conditions on the four side walls with master-slave boundary conditions, as shown in Fig. 8(a), where the  $E$ -field at every point on the slave boundary surface is forced to match the  $E$ -field of every corresponding point on the master boundary surface to within phase difference  $\Phi$ ,



(a)



(b)

FIG. 7. Reflection-phase characteristics of oblique incidence plane waves on PBG structure without vias: (a) TM-polarized plane waves; (b) TE-polarized plane waves.

$$\mathbf{E}_S = e^{j(\boldsymbol{\beta} \cdot \mathbf{a})} \mathbf{E}_M = e^{j\Phi} \mathbf{E}_M, \quad (5)$$

where  $\mathbf{a}$  represents a lattice vector of the PBG structure and  $\boldsymbol{\beta}$  denotes a wave vector of propagation along the PBG surface. The modified LRCC model can be used to analyze the dependence of mode resonance frequencies on the incidence angle and plane-wave polarization. Assume the relative phase between the master and slave boundary walls is  $\Phi_x = 40^\circ$  in the  $x$ -direction and  $\Phi_y = 0^\circ$  in the  $y$ -direction. The relative phase difference can be used to represent the phase delay due to plane-wave oblique incidence at the  $xz$  plane. The eigenmodes supported by the MLRCC model were computed using the HFSS EIGENMODE SOLVER. Figures 8(b)–8(e) show the normalized three-dimensional  $E$ -field distribution for the lower four modes in the cavity. The vector  $E$ -fields on the cavity walls with the master-slave boundaries are also shown to distinguish the polarization modes. In terms of the phase difference, we used the  $xz$  plane as the reference “plane of incidence.” Mode 1 is TM polarization that has  $E_x$  and  $E_z$  components, i.e.,  $\mathbf{E}_{\text{mode 1}}$  lying in the plane of incidence. Mode 2 is TE polarization that has only an  $E_y$  component, i.e.,  $\mathbf{E}_{\text{mode 2}}$  perpendicular to the plane of incidence. Mode 3 is TM polarization, which has an  $E$ -field distribution similar to that of mode 1, which contributes to the second resonance. Mode 4 is a higher-order mode that has a com-

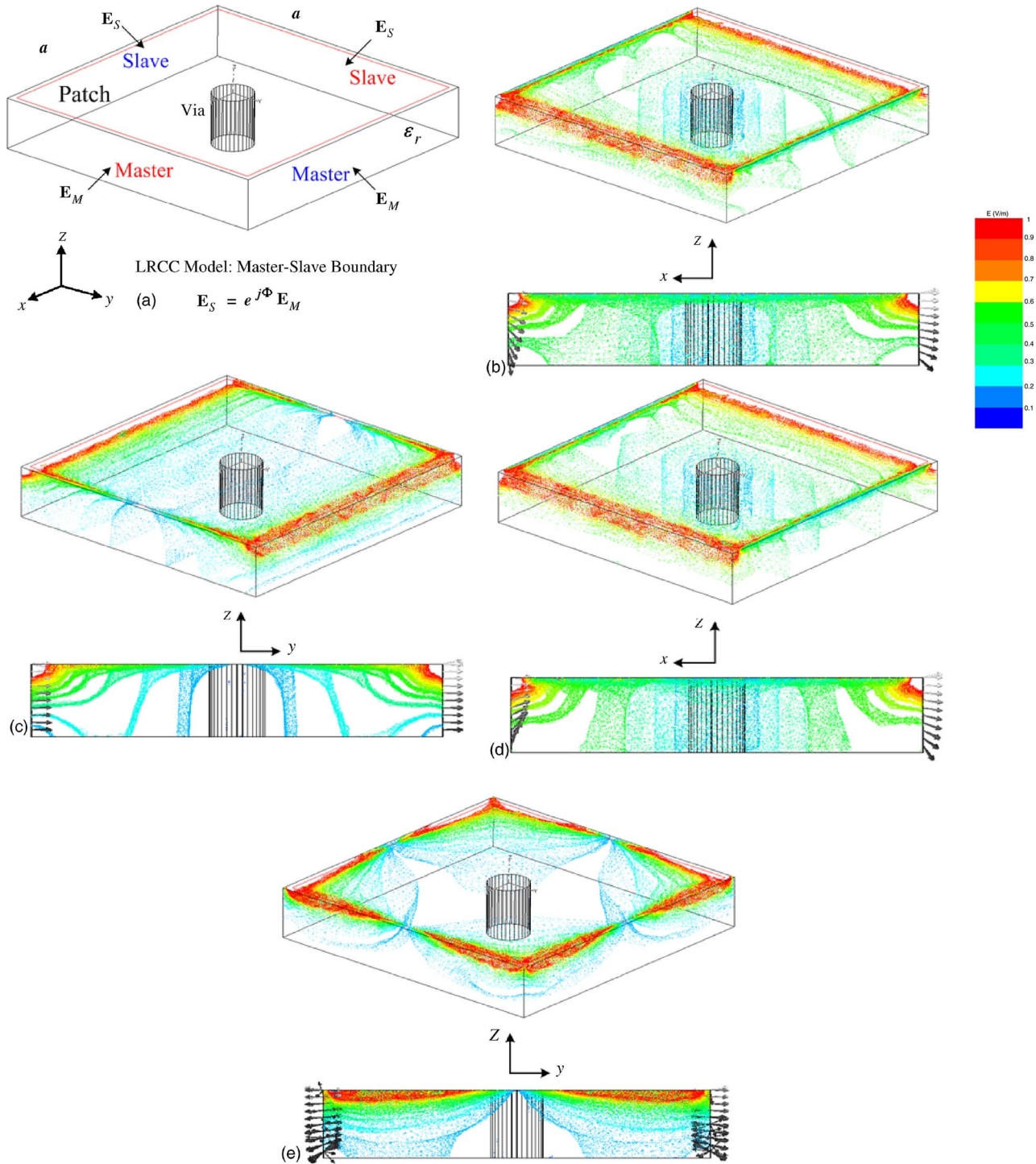


FIG. 8. (Color online) (a) Modified LRCC model of mushroomlike PBG structure with master-slave boundary. Normalized three-dimensional  $E$ -field distribution for lower four modes in cavity: (b) Mode 1 ( $f_1=7.622$  GHz), TM-polarization; (c) Mode 2 ( $f_2=8.919$  GHz), TE-polarization; (d) Mode 3 ( $f_3=9.683$  GHz), TM-polarization; and (e) Mode 4 ( $f_4=15.17$  GHz), higher-order mode.

plex polarization and is difficult to excite. When a TM-polarized plane wave obliquely illuminates the PBG structure, as shown in Fig. 5, the incident TM electric field can excite both modes 1 and 3 at different resonant frequencies, which results in the dual in-phase reflection phenomenon. When a TE-polarized plane wave obliquely illuminates the structure, the incident TE electric field excites only mode 2 and produces an in-phase reflection band.

By analyzing the resonant frequencies of the three domi-

nant modes supported by the MLRCC model in comparison to the relative phase differences between the cavity walls in the  $x$ -direction, we obtained the dependence characteristics of plane-wave incidence angle  $\theta$  based on the transverse phase matching condition,<sup>22</sup> as shown in Fig. 9(a). When the transverse phase matching condition,  $ka \sin \theta = \beta a = \Phi$ , is achieved, resonant modes 1 and 3 are excited by a TM-polarized plane wave at the same incident angle, and the resonant mode 2 is excited by a TE-polarized plane wave at

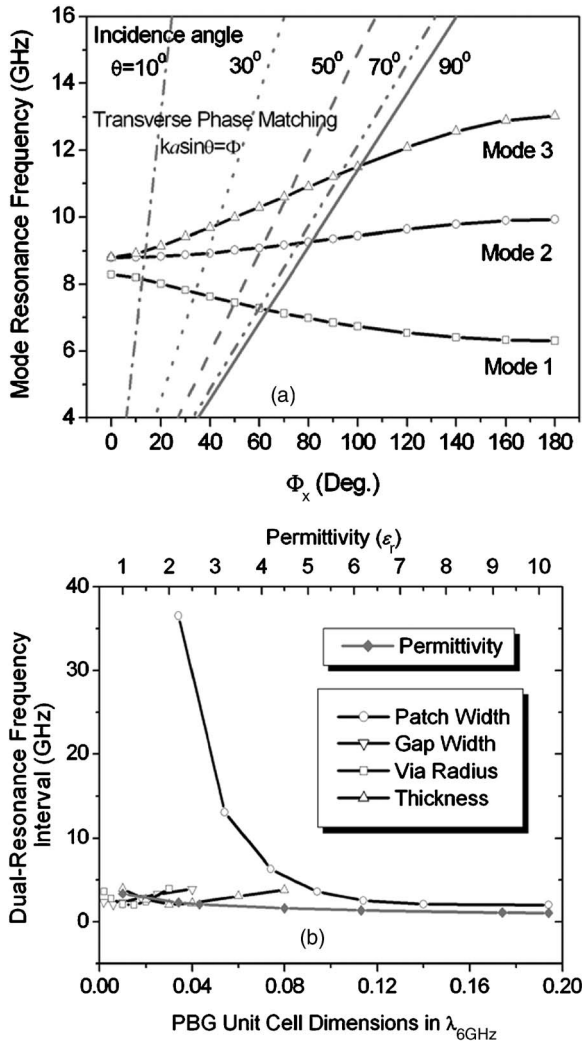


FIG. 9. (a) Mode resonant frequencies of MLRCC model vs relative phase difference between master and slave boundaries, in which oblique lines correspond to the transverse phase matching conditions of plane-wave excitation at different incidence angles. (b) Curves showing variation in frequency interval between first and second TM resonance vs PBG unit cell dimensions (for  $\Phi_x=40^\circ$ ).

the same incident angle. The curves in Fig. 9(b) show the variation in the frequency distance between the first and second TM resonances versus the PBG unit cell dimensions, assuming  $\Phi_x=40^\circ$ . It can be seen that the second resonance also exists in the other mushroomlike PBG structures previously investigated,<sup>15,20,21</sup> for which only a single resonance band was indicated for an obliquely incident TM wave. The second resonance mode (mode 3) was excited but was far from the first in-phase band, so the corresponding resonance behavior was not observed. Our analyses using the MLRCC model showed that the frequency interval between the first and second TM resonances rapidly decreased as the patch size was increased, and that the dual-resonance frequency interval increased as the incidence angle was increased, as illustrated in Fig. 6(a). Nevertheless, this dual-resonant behavior of the PBG structure should have some application. Mode analysis using the MLRCC model for a PBG structure without vias showed that resonant mode 3 does not exist if the effective cavity had no metal vias. Therefore, only a

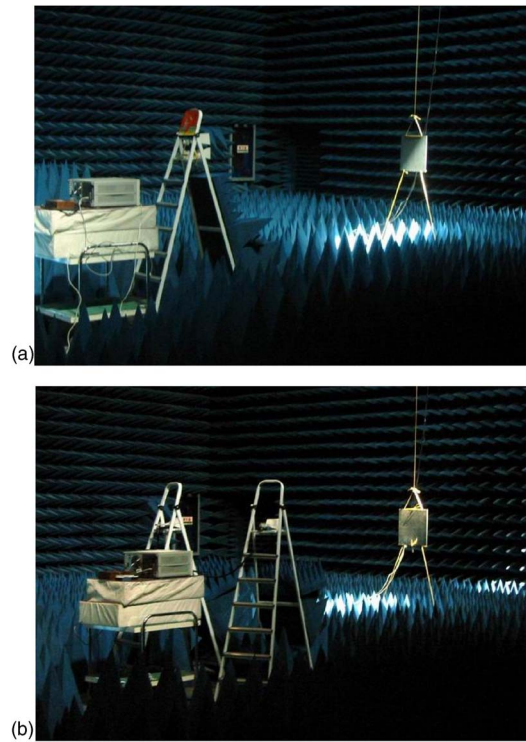


FIG. 10. (Color online) Setups used for measuring reflection phase with a pair of wideband horn antennas in an anechoic chamber for (a) normal incidence and (b) oblique incidence.

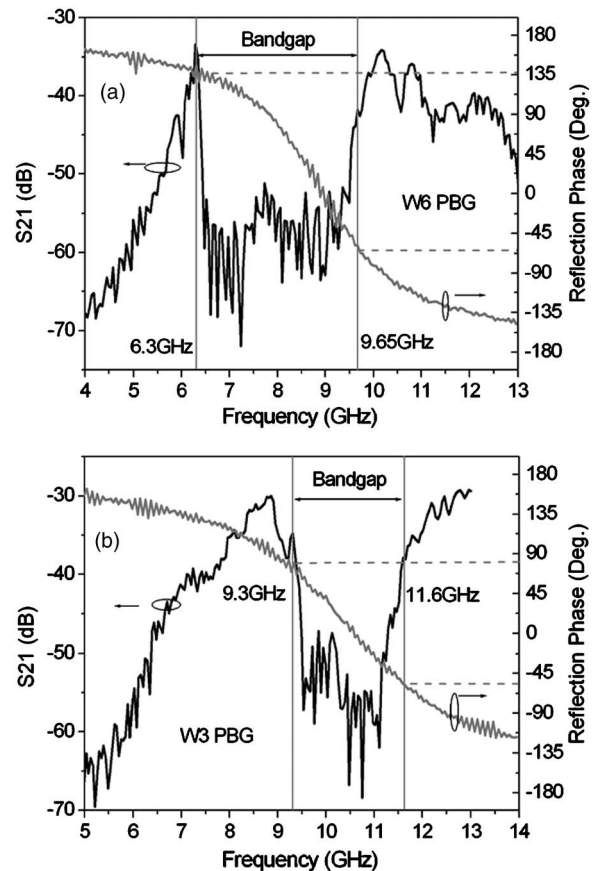


FIG. 11. Measured surface-wave band gap and measured plane-wave reflection phase band: (a) W6 PBG structure with  $a/t=4.0$  and (b) W3 PBG structure with  $a/t=2.0$ .

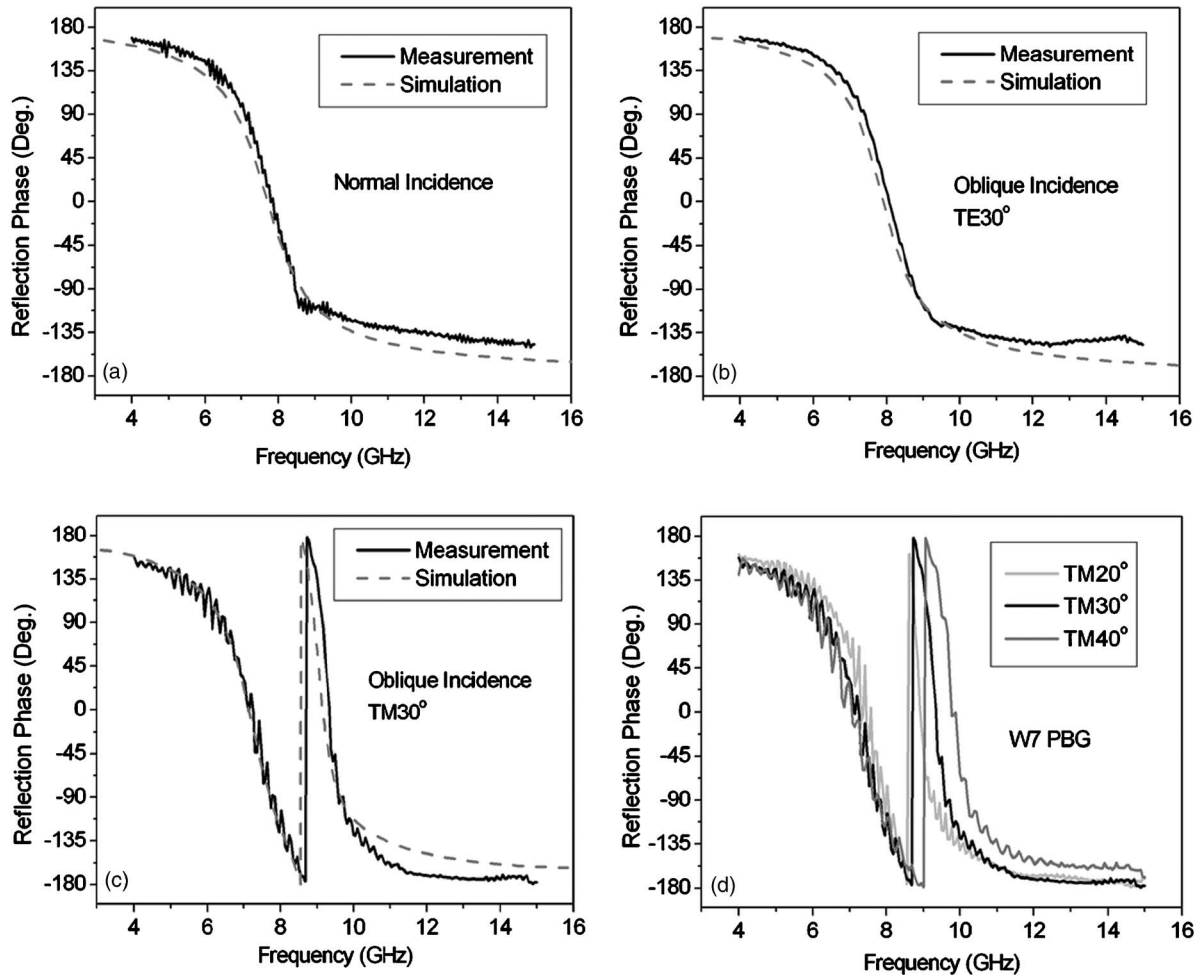


FIG. 12. Measured and simulated reflection phases of PBG structure: (a) plane wave at normal incidence; (b) TE-polarized plane wave at oblique incidence ( $30^\circ$ ); (c) TM-polarized plane wave at oblique incidence ( $30^\circ$ ); and (d) TM-polarized plane waves at oblique incidences ( $20^\circ$ ,  $30^\circ$ , and  $40^\circ$ ).

single in-phase reflection band can be found when a TM- or TE-polarized plane wave is obliquely incident on a PBG structure without vias.

## V. EXPERIMENTAL VERIFICATION

We experimentally verified the results obtained by numerical simulation, especially the relationship between the surface-wave suppression band gap and the plane-wave in-phase reflection band. Two mushroomlike PBG plates with different dimensions and substrate materials (CGP-500 and CGK-500) were fabricated. One plate (W6) was  $268.8 \times 268.8$  mm, i.e.,  $42 \times 42$  cells, with  $W=6.0$ ,  $g=0.4$ ,  $t=1.6$ , and  $r=0.4$  mm,  $\epsilon_r=2.6$  (CGP-500), and  $a/t=4.0$ . The other plate (W3) was  $256 \times 256$  mm, i.e.,  $80 \times 80$  cells, with  $W=2.84$ ,  $g=0.36$ ,  $t=1.6$ , and  $r=0.4$  mm,  $\epsilon_r=5.0$  (CGK-500), and  $a/t=2.0$ . The results of our numerical calculations indicate that the surface-wave band gap of the W3 PBG corresponds to its in-phase reflection band and that of the W6 PBG does not. The surface-wave band gap was measured using a pair of small shielded loop antennas parallel to the PBG surface. From the results shown in Fig. 3(b), we know that the loop probes used in a TE surface-wave experiment also couple to the TM surface wave, so the TM band edge is reflected in this measurement.

Bistatic reflection experiments were conducted using the far-field measurement technique for the reflection phase. Two wideband horn antennas were carefully aligned with the center of the PBG plate. An absorber was placed between the horns to reduce spillover and mutual coupling. An Agilent 8722ET transmission/reflection network analyzer was used to measure the reflection phase, and the ratio calibration method was used to eliminate such errors as phase and amplitude taper and edge scattering due to finite sample size. A metal calibration plate the same size as the PBG sample was used to normalize the test sample reflection measurement. Figures 10(a) and 10(b) show the setups used for measuring the reflection phase in an anechoic chamber for normal and oblique incidences, respectively.

The measured surface-wave band gaps and plane-wave reflection phase bands for the W6 and W3 PBG plates are shown in Figs. 11(a) and 11(b), respectively. The results further validate the theoretical analysis. When the period-to-thickness ratio was less than 2, the surface-wave band gap corresponded to its in-phase reflection band, as expected.

To verify the dual in-phase reflection, we used the experimental setup for oblique incidence shown in Fig. 10(b). The polarization was determined by the  $E$ -field orientation. When the horn antennas were set for vertical polarization, i.e., the  $E$ -field was vertical with respect to the floor, the

plane wave was transverse-electric polarized. When the horns were set for horizontal polarization, the plane wave was transverse-magnetic polarized. The illumination angle was with respect to the normal of the PBG surface. The size of the PBG plate (W7) was  $365 \times 365$  mm, i.e.,  $50 \times 50$  cells, with  $W=7.0$ ,  $g=0.3$ ,  $t=1.5$ , and  $r=0.5$  mm and  $\epsilon_r=2.65$ . Comparing the measured results with the simulated ones, as shown in Figs. 12(a)–12(d), we can see that the simulation results are in good agreement with the experimental ones. The dual in-phase reflection phenomenon was observed when the TM polarization plane wave obliquely illuminated the PBG plate.

## VI. CONCLUSION

We investigated the surface-wave suppression band gap and the plane-wave reflection phase properties of mushroom-like PBG structures to clarify the relationship between the two bands. A parametric study revealed that the period-to-thickness ratio plays an important role in adjusting the simultaneous appearance of the surface-wave suppression band gap and the plane-wave in-phase reflection band.

The reflection phase characteristics of plane waves normally and obliquely illuminating a mushroomlike PBG structure have been investigated by simulations and experiments in this paper. We found that dual in-phase reflection bands can be obtained when a TM-polarized plane wave obliquely illuminates the PBG surface. A local resonance cavity cell model of the PBG structure shows that this can be attributed to the incident TM electric field exciting the metal vias and coupling the two resonance modes.

## ACKNOWLEDGMENTS

This work is partially supported by the National Natural Science Foundation of China under Contract No. 60601028,

and partially supported by JSPS Postdoctoral Fellowship of Japan.

- <sup>1</sup>E. Yablonovitch, Phys. Rev. Lett. **58**, 2059 (1987).
- <sup>2</sup>S. John, Phys. Rev. Lett. **58**, 2486 (1987).
- <sup>3</sup>S. G. Johnson and J. D. Joannopoulos, *Photonic Crystals – The Road from Theory to Practice* (Kluwer Academic, Dordrecht, 2002).
- <sup>4</sup>J. B. Pendry, Phys. Rev. Lett. **85**, 3966 (2000).
- <sup>5</sup>R. A. Shelby, D. R. Smith, and S. Schultz, Science **292**, 77 (2001).
- <sup>6</sup>F. R. Yang, K. P. Ma, Y. Qian, and T. Itoh, IEEE Trans. Microw. Theory Tech. **47**, 1509 (1999).
- <sup>7</sup>D. Sievenpiper, L. Zhang, R. F. J. Broas, N. G. Alexopolus, and E. Yablonovitch, IEEE Trans. Microw. Theory Tech. **47**, 2059 (1999).
- <sup>8</sup>L. Li, B. Li, H. X. Liu, and C. H. Liang, IEEE Trans. Antenn. Propag. **54**, 90 (2006).
- <sup>9</sup>F. Yang and Y. Rahmat-Samii, IEEE Trans. Antenn. Propag. **51**, 2939 (2003).
- <sup>10</sup>Z. Iluz, R. Shavit, and R. Bauer, IEEE Trans. Antenn. Propag. **52**, 1446 (2004).
- <sup>11</sup>L. Zhang, J. A. Castaneda, and N. G. Alexopoulos, IEEE Trans. Antenn. Propag. **52**, 2000 (2004).
- <sup>12</sup>T. H. Liu, W. X. Zhang, M. Zhang, and K. F. Tsang, Electron. Lett. **36**, 779 (2000).
- <sup>13</sup>F. Yang and Y. Rahmat-Samii, IEEE Trans. Antenn. Propag. **51**, 2691 (2003).
- <sup>14</sup>S. Clavijo, R. E. Diaz, and W. E. McKinzie, IEEE Trans. Antenn. Propag. **51**, 2678 (2003).
- <sup>15</sup>S. A. Tretyakov and C. R. Simovski, J. Electromagn. Waves Appl. **17**, 131 (2003).
- <sup>16</sup>M. A. Saville, “Investigation of Conformal High-Impedance Ground Planes,” M.Sc. thesis, Air Force Institute of Technology, 2000.
- <sup>17</sup>R. Remski, Microwave J. **43**, 190 (2000).
- <sup>18</sup>S. A. Tretyakov, *Analytical Modeling in Applied Electromagnetics* (Artech House, Norwood, MA, 2003).
- <sup>19</sup>J. R. Wait, Can. J. Phys. **32**, 571 (1954).
- <sup>20</sup>C. R. Simovski, P. de Maagt, S. A. Tretyakov, M. Paquay, and A. A. Sochava, Electron. Lett. **40**, 92 (2004).
- <sup>21</sup>C. R. Simovski, P. de Maagt, and I. V. Melchakova, IEEE Trans. Antenn. Propag. **53**, 908 (2005).
- <sup>22</sup>A. R. Cowan and J. F. Young, Phys. Rev. B **65**, 085106 (2002).